DOI: 10.1002/((please add manuscript number))

Article type: Full Paper

Erythrocyte-Derived Nanoparticles as a Theranostic Agent for Near Infrared Fluorescence Imaging and Thrombolysis of Blood Clots

Raviraj Vankayala[a], Samantha R. Corber[b], Jenny T. Mac[c], Masaru P. Rao[a,b,d], Mohammad Shafie[e], Bahman Anvari[a,b,c]*

[a]Dr. Raviraj Vankayala, Prof. Bahman Anvari, Prof. Masaru P. Rao

Department of Bioengineering, University of California, Riverside,

900 University Avenue, Riverside CA 92521, USA
E-mail: bahman.anvari@ucr.edu

[b]Samantha R. Corber, Prof. Masaru P. Rao

Department of Mechanical Engineering, University of California, Riverside,

900 University Avenue, Riverside CA 92521, USA

[c]Jenny T. Mac

Department of Biochemistry, University of California, Riverside,

900 University Avenue, Riverside CA 92521, USA

[d]Prof. Masaru P. Rao

Materials Science and Engineering Program, University of California, Riverside,

900 University Avenue, Riverside CA 92521, USA

[e]Prof. Mohammad Shafie

School of Medicine, Department of Neurology, University of California, Irvine,

200 S. Manchester Ave. Ste 206, Orange, CA 92868, USA

Keywords: drug delivery, indocyanine green, ischemic stroke, targeting, tissue plasminogen activator

Abstract: Ischemic stroke occurs when a blood clot obstructs or narrows the arteries that supply blood to the brain. Currently, tissue plasminogen activator (tPA), a thrombolytic agent, is the only United States Food and Drug Administration (FDA)-approved pharmacologic treatment for ischemic stroke. Despite its effective usage, that major limitations of tPA that stem from its short half-life in plasma (~5 minutes) and non-specific uptake by other organs, can lead to potential increased risk of hemorrhagic complications. To circumvent these limitations, herein, we report the first proof-of-principle demonstration of a theranostic nano-construct system derived from erythrocytes doped with the FDA-approved near infrared (NIR) imaging agent, indocyanine green, and surface-functionalized with tissue plasminogen activator. Using a clot model, we demonstrate the dual functionality of these nano-constructs in NIR fluorescence imaging and clot lysis. These biomimetic theranostic nano-constructs may ultimately be effective in imaging and treatment of blood clots involved in ischemic stroke.

1. Introduction

Ischemic stroke is one of the leading causes of death and long-term disability in the world.[1] The mechanisms of ischemic stroke are heterogeneous; however, the underlying pathology involves occlusive thrombosis in a cerebral vessel leading to obstruction of blood flow. The current proven treatment of ischemic stroke entails restoring cerebral blood flow and reperfusion of at-risk brain tissue through either pharmacologic or mechanical means. Tissue plasminogen activator (tPA) is the only existing Food and Drug Administration (FDA)-approved pharmacologic treatment for ischemic stroke,[2] and is systemically administered by intravenous (IV) injection. It is a naturally occurring enzyme that catalyzes the conversion of plasminogen to plasmin when bound to fibrin in blood clots, resulting in dissolution of clots. Since IV-administered tPA is less effective on larger more proximal clots and better suited at dissolving smaller distal clots, endovascular therapies, whereby mechanical devices are delivered via catheter angiography to remove the clot and restore blood flow in the blocked cerebral artery, have evolved as an additional treatment option for ischemic stroke. Recent successful clinical trials have established endovascular therapies either in combination with IV-administered tPA, or solely on their own in carefully selected patients as an additional standard treatment option for ischemic stroke.[2]

However, reperfusion therapies for ischemic stroke are time-dependent and can only be implemented within the first few hours (typically 3-6 hours) from onset of stroke symptoms. Reperfusion therapies even when administered within this narrow therapeutic time window are not risk-free, and are associated with a recognized risk of intracerebral hemorrhage (ICH) and ischemic-reperfusion injury. In case of tPA, ICH occurs, at least partly, due to the very short half-life of tPA in plasma requiring administration at high doses for prolonged period of time

to maintain effective therapeutic levels. Similar to tPA, endovascular treatments with catheter-delivered devices are not risk-free, and are susceptible to hemorrhagic complications and prone to additional concerns such as vessel perforation, distal embolization with new subsequent ischemic stroke in a different vascular territory after the initial stroke. Furthermore, these interventional approaches and their implementation requirements of extremely specialized resource-intensive hospital setting limit their utilization.

To overcome these limitations and improve the therapeutic outcomes, several attempts have been made to encapsulate or chemically conjugate tPA molecules and target clots. Various approaches such as those based on the use of small peptide molecules, or mediated by electrostatic interactions or stimuli-induced release by shear stress or ultrasound have been investigated.[3-7] For example, biocompatible and biodegradable microaggregates of poly (lactic-co-glycolic acid) nanoparticles have been coated with tPA using biotin-streptavidin chemistry, and evaluated for their ability to dissolve clots.[5] Recently, clustered superparamagnetic iron oxide nanocubes stabilized by surface coating with tPA and serum albumin were used as vascular thrombolytic agents with alternating magnetic field as an external stimulus.[8] Although these approaches have demonstrated an improved clot dissolution rate of tPA, delivery of adequate levels of tPA molecules to the occlusive clot still remains as a major constraint for ultimate clinical translation.

Apart from liposomes,[4] synthetic polymers,[5] and magnetic nanoparticles,[8] attention has also been given to the use of biological materials such as erythrocytes as carriers for the delivery of therapeutic payloads to target sites.[9-12] One feature of normal erythrocytes is their naturally long circulation time (≈ 90-120 days), attributed to the presence of "self-marker" proteins on their surface.[13] Owing to this feature,

constructs derived from erythrocytes may offer a promising approach for increased circulation time of their payload within the vasculature.[14,15] Previously, tPA molecules were conjugated on the surface of erythrocytes via biotin-streptavidin chemistry for blood clot lysis.[9-10,16] We have fabricated constructs derived from nano-sized erythrocyte ghosts (EGs), which can be doped with imaging and/or therapeutic agents, referred as NETs (NIR erythrocyte-derived transducers).[11,12] NETs offer dual functionality for NIR imaging by encapsulating indocyanine green (ICG), and therapeutic capability by covalent attachment of tPA, as thrombolytic agent, to its surface. The constructs referred to as tPA-conjugated NETs may offer prolonged circulation times when compared to free tPA, permitting the use of tPA at lowered dosages.

We note that this is not an in vivo study. Instead, to the best of our knowledge, we report the first study to demonstrate the successful engineering of tPA-conjugated erythrocyte-derived nanoparticles, and evaluating their potential utility as theranostic agents for imaging and dissolution of blood clots in a model system. Results of this study provide the basis towards further development and engineering of this theranostic nanoplatform with optimized concentration of ICG and photo-excitation wavelengths for maximal fluorescence emission, as well as optimized tPA concentration for maximal lysis activity prior to further animal studies to ultimately tackle thrombolytic disease.

2. Results and Discussion

A schematic representation of the fabrication of tPA-conjugated NETs is shown in **Figure 1**. It depicts the insertion of the lipid linker molecule, 1,2-distearoyl-sn-glycero-3-

phosphoethanolamine-polyethylene glycol-aldehyde group (DSPE-PEG-CHO) into the membrane of erythrocyte ghosts (EGs) followed by mechanical extrusion to obtain nano-sized EGs.[12] These nano-sized EGs were subsequently loaded with NIR imaging agent, ICG, in a hypotonic solution and then conjugated with tPA via amine-aldehyde chemistry to create a theranostic nano-platform with imaging and therapeutic capabilities. The estimated mean peak values of hydrodynamic diameters for NETs and tPA-conjugated NETs, as estimated by dynamic light scattering (DLS), were ~122 nm and ~190 nm, respectively (**Figure 2a**). Therefore, grafting the DSPE-PEG-CHO linker and tPA on NETs increased the mean peak diameter of such functionalized NETs by ≈ 68 nm. This increase in diameter corresponds to coating thickness of 34 nm associated with the presence of DSPE-PEG-CHO and tPA. Using differential centrifugal sedimentation methods, Minelli and Shard have estimated the thickness of PEG coatings of various molecular weights on the surface of gold nanoparticles.[17] Based on our extrapolation of their data, we estimate the thickness of the 2kDa PEG component of linker structure connecting tPA to surface of NETs to be ≈ 19 nm. Additionally, a reported thickness of tPA monolayer is ≈ 6 nm.[3] Therefore, our estimated mean peak thickness of ≈ 34 nm for the graft is a reasonable value considering the estimated thicknesses of some of the individual components.

The polydispersibility index (PDI) values of NETs and tPA-conjugated NETs were 0.205 and 0.262 respectively, which indicates that particle suspensions are moderately polydispersed since the respective PDI values are in the range of 0.1~0.4.[18] The mean ± standard deviation (SD) zeta-potential values for red blood cells (RBCs), EGs, NETs and tPA-conjugated NETs formulations in 1× (≈ 310 mOsm) phosphate buffer saline (PBS) (pH ~ 7.4) were -11.4 ± 1.4, -11.5 ± 2.2, -12.0 ± 1.5 and -17.5 ± 2.5 mV respectively (Figure 2b). The negative potential can

arise from the anionic phospholipids, and surface-bound negatively charged membrane proteins, or ICG embedded within the membrane. These results suggest that after lipid insertion, extrusion, and ICG loading, some of the constituent membrane molecules remain embedded to contribute to the resulting negative zeta potential. A statistically significant increase in the net negative zeta-potential value was observed for tPA-conjugated NETs compared to that of NETs, which can be attributed due to the presence of negatively charged amino acid residues on the tPA molecules. This result is an indication of successful functionalization of tPA molecules on the surface of NETs.

Absorption and fluorescence spectral characteristics of NETs and tPA-conjugated NETs are shown in **Figure 3**. The peak absorption of free tPA at 280 nm is consistent with the presence of the amino acid residues in the protein. The absorbance value at 280 nm for NETs corresponds to the membrane proteins present on the surface of erythrocytes. Absorbance value at 280 nm increased from ≈ 1.16 for NETs to ≈ 1.43 for tPA-conjugated NETs (Figure 3a), suggesting that tPA was successfully conjugated on the surface of NETs. These results are also consistent with the increase in the mean peak diameter of tPA-conjugated with a coating thickness of ≈ 34 nm.

The absorption spectrum of NETs and tPA-conjugated NETs dissolved in PBS showed a peak at 803 nm, which is attributed to the monomeric form of ICG.[11,19] The absorption spectrum of the supernatant showed reduced absorption at 280 nm, indicating that most of the tPA molecules were grafted to the surface of NETs. In addition, small absorption of the supernatant at 790 nm can be attributed to the ICG molecules, which were not incorporated into the NETs. The fluorescence emission spectra of NETs and tPA-conjugated NETs in response to 720 nm excitation wavelength were similar, and showed a peak at 793 nm but with

a more intense emission at this spectral peak for NETs (Figure 3b). To evaluate the imaging capabilities of NETs*, in vitro* clot models were exposed to free tPA, NETs and tPA-conjugated NETs in PBS solution for one hour, and the fluorescence emitted by ICG, were then recorded following incubation (**Figure 4a**). Clots exposed to tPA-conjugated NETs showed higher fluorescence signal compared to those exposed to NETs; blood clots exposed to free tPA did not show any noticeable fluorescence. These findings indicate that tPA-conjugated NETs can effectively bind to the fibrin of the blood clot. Using these images, we determined the averaged total emission intensity (I^*) from the blood clots and found a statistically significant higher value associated with tPA-conjugated NETs as compared to that of NETs ($p < 0.05$) (Figure 4b).

To further evaluate the capability of tPA-conjugated NETs binding to *in vitro* model clots, we incubated the clots with PBS, NETs and tPA-conjugated and imaged them by confocal fluorescence microscopy (**Figure 5**). While fibrin networks were clearly visualized in all blood clots, the respective clots incubated with PBS and NETs showed none and minimal NIR fluorescence associated with ICG after 30 minutes of incubation (Figures 5a and 5b). Upon treatment with tPA-conjugated NETs, NIR fluorescence emission from the model blood clot was enhanced (Figure 5c), indicating that the tPA-conjugated NETs were effective in binding or interacting with clot-associated fibrin network. Imaging using tPA conjugated-NETs was still possible despite the fact that a non-optimal excitation wavelength of 633 nm, where there is relatively low absorption by ICG (Figure 3a), was utilized in the confocal system.

To evaluate clot lysis efficacies, *in vitro* model clots were exposed to the thrombolytic agents in PBS solution. In control experiments, model clots were only incubated in PBS (Figure **6a**) The degree of clot dissolution at 0 and 120 minutes post-incubation with tPA-conjugated NETs (fabricated using 61.25 and 125 μg/ml of tPA in the reaction buffer) and free

tPA (50 and 100 μg/ml) were evaluated. Representative images demonstrate that tPA-conjugated NETs were effective in lysis of clots (Figures 6b&c). The amount of lysed clot, was determined as the difference in clot mass between the 0 and 120 min post-incubation (Figure 6d). We note that there is tPA loss during the conjugation process of NETs, making the effective concentration of the conjugated tPA is lower than that of the tPA concentration introduced in the reaction buffer. Effective conjugated concentration of tPA would be concentration if all tPA molecules were to be fully detached from NETs. Loss of tPA during the conjugation process is evident from the absorption spectra shown in Figure 3a. Based on the respective absorbance values of tPA in supernatant and tPA-conjugated NETs (Figure 3a), we estimate tPA loss of ≈ 11% during the fabrication process of these conjugated NETs. Therefore, the effective concentration of tPA conjugated on NETs fabricated from 125 μg/ml of tPA in reaction buffer would be ≈ 111 μg/ml. The statistically significant higher thrombolytic activity of tPA-conjugated NETs fabricated using 125 μg/ml of tPA in reaction buffer as compared with those by free tPA (Figure 6d) can be attributed to the higher effective concentration of tPA molecules conjugated on NETs. Similarly, the lower thrombolytic activity of tPA-conjugated NETs fabricated from 61.25 μg/ml of tPA in the reaction buffer as compared to those by free tPA may be due to the effective conjugated tPA concentration of less than 50 μg/ml. This reduced effective concentration may have resulted from tPA loss of greater than 11% when fabricating these particular tPA-conjugated NETs.

In general, the therapeutic potential of free tPA is severely hindered due to its rapid clearance from the bloodstream within minutes. To overcome this limitation, in clinical setting, excessive dosage of free tPA is usually administered. However, elevated dosages are associated with neuronal toxicity and risk of bleeding. Alternatively, various delivery systems, including liposomal-tPA delivery systems have been designed to improve the bioavailability

of tPA.[4-12] However owing to its instability in the bloodstream and poor clot lysis efficiencies, practical application of liposomal delivery systems is restricted.[21,22]

It has been reported that upon bolus injection, native RBCs attached to tPA show longer circulation (up to 2 hours) than free tPA in the bloodstream without any haemolysis of the carrier RBCs.[9] The major potential advantages of tPA-conjugated NETs used in this study, as compared to other types of tPA delivery systems are their expected biocompatibility and safety, and the presence of ICG to achieve theranostic functions. It is important to note that the tPA molecules could still activate the fibrinolytic process while conjugated on the surface of NETs. Unlike liposomal-tPA delivery systems, there is no necessity for tPA to be detached from the nano-constructs to induce thrombolytic activity.[21] In addition, tPA-conjugated NETs could potentially show less risk of bleeding when compared to free tPA.

tPA-based particle delivery systems can specifically target the fibrin molecule of the blood clots, as the epitope components of fibrin are exposed, and often viewed as a molecular target for selective delivery of thrombolytic agents to the thrombi. For example, nanocomposites containing iron oxide nanoparticles and urokinase-type plasminogen activator (uPA) have been developed as magnetically targetable thrombolytic agents for the treatment of blood clots, and demonstrated clot lysis efficacy. Due to its nanoporous architecture of the composite material, the entrapped urokinase can interact with plasminogen to convert to plasmin, and also prevent the release of urokinase from a magnetite matrix.[23] In another study, a biophysical targeting strategy was adopted to break the microscale aggregates of nanoparticles into nanoscale components when exposed to abnormally high fluid shear stresses due to the narrowing of the vasculature. Upon coating with tPA and systemic administration into mice, these shear-activated nanotherapeutics induced rapid clot dissolution in a mesenteric injury

model, restored normal flow dynamics, and increased survival in an otherwise fatal mouse pulmonary embolism model.[24]

In an illustrative *in vivo* experiment using mice with average weight of ≈ 20 g, the injection volume would be ≈ 0.1 ml. Under this scenario, an example dosage of tPA administered to an animal as a conjugated-NETs formulation would be (111 μg/ml x 0.1 ml)/20 g ≈ 0.55 μg/g, or ≈ 0.55 mg/kg. Based on the scaling factor of 0.081 to convert the mouse dosage to human equivalent dosage (HED)[25], our estimated HED for tPA in conjugated-NETs formulation would be ≈ 0.04 mg/kg, which is ≈ 22 times lower than the recommended free tPA dosage of 0.9 mg/kg.[26] Future studies will be aimed at optimizing the respective concentrations of ICG and tPA for maximal fluorescence emission and thrombolytic activity, and evaluating efficacy and toxicity in relevant animal models.

3. Conclusions

We report the first proof-of-principle demonstration of thrombolysis using a new theranostic nanoplatform system. The nano-structured system is comprised of vesicles derived from erythrocytes that encapsulate the FDA-approved NIR fluorophore, ICG, and are conjugated at the surface with the FDA-approved thrombolytic agent, tPA. Our results demonstrate the effectiveness of these constructs for NIR fluorescence imaging and thrombolysis of model blood clots. Future experiments will explore the *in vivo* use of tPA-conjugated NETs for fluorescence imaging-guided clot lysis in a mouse stroke model.

4. Experimental Section

4.1. NETs fabrication and conjugation with tPA

Erythrocytes were separated from bovine whole blood (Rockland Immunochemicals, Inc., Limerick, PA) by centrifugation process. In a typical experiment, 10 ml of bovine whole blood was taken in an

eppendorf, and centrifuged for 10 minutes at 1600×g at 4 °C. The supernatant containing the plasma and buffy coat were discarded, and the resulting packed erythrocytes were washed twice with 1X (≈ 310 mOsm, pH ~ 8.0) phosphate buffer solution (PBS). The erythrocytes were then subjected to sequential hypotonic treatment with 0.5X (≈ 155 mOsm, pH ~ 8.0) and 0.25X (≈ 80 mOsm, pH ~ 8.0) PBS, and centrifuged (20,000×g; 10 min; 4 °C) until nearly all the hemoglobin was depleted, resulting in an opaque white pellet. The obtained pellet containing micron-sized hemoglobin-depleted erythrocyte ghosts (EGs) were re-suspended in 1 ml of 1X PBS.

To covalently conjugate tPA molecules to the surface of NETs, a lipid linker molecule, 1,2-distearoyl-sn-glycero-3-phosphoethanolamine-polyethylene glycol-aldehyde group (DSPE-PEG-CHO) (5 kDa, Nancos, Inc, New York, NY) was used to connect the surface of EGs through lipid insertion mechanism in water followed by filtration and exchange of buffer to 1X PBS through 50k Amicon Ultra-centrifuge units. To obtain nano-sized EGs, the micron-sized EGs bearing lipid inserted DSPE-PEG-CHO were extruded 20 times through 400 nm polycarbonate porous membranes, followed by 20 more extrusions through 100 nm polycarbonate porous membranes using an extruder (Avanti mini extruder, Alabaster, Alabama).

To load ICG into nano-sized EGs, 350 µl of nano-sized EGs suspended in PBS were incubated with 23 µl of ICG stock solution (645 µM), 350 µl of hypotonic buffer (Na_2HPO_4/NaH_2PO_4, 140 mOsm, pH ~8.0) and 280 µl nanopure water for 5 minutes at 4 °C in the dark. The concentration of ICG in this loading buffer was 15 µM. The suspension was then centrifuged and washed twice with 1X PBS 100,000×g for 30 minutes. These NETs bearing lipid inserted DSPE-PEG-CHO were re-suspended in 1X cold PBS buffer solution to restore tonicity.

We incubated a mixture of 870 µl of NETs bearing lipid inserted DSPE-PEG-CHO (2 kDa, Nancos, USA), 5 µl of 20 mM sodium dithionite dissolved in in water, 61.25 or 125 µg/ml of human tissue plasminogen activator (65 kDa, Sigma-Aldrich, USA) for 60 minutes at 4 °C in the dark. The reaction between the aldehyde group and the α-amine at the N-terminus produces an intermediate Schiff base. Further reduction with sodium dithionite results in a stable C-N bond. After incubation, the suspension was then centrifuged and washed twice with 1X PBS 100,000×g for 30 minutes and then re-suspended in 1 ml of 1X cold PBS buffer solution.

4.2. Characterization of NETs

The absorption spectra of free tPA, NETs and tPA-conjugated NETs suspended in 1X PBS were obtained using a UV-visible spectrophotometer (Cary 50, Varian Inc., Santa Clara, CA, USA) with optical path length of 1 cm. The fluorescence emission spectra of NETs in response to 720 nm excitation with a 450 W xenon lamp were recorded using a fluorimeter (Fluorolog-3, Horiba−Jobin-Yvon, Inc., Edison, NJ, USA). Normalized fluorescence emission spectra (ζ) were defined as:

$$\zeta(\lambda) = \frac{F(\lambda)}{1-10^{-A(\lambda_{ex})}} \quad (1)$$

where *A* and *F* are the wavelength (λ) dependent absorbance and intensity of the emitted fluorescence light, respectively, and λ_{ex} is the excitation wavelength. The hydrodynamic diameters and zeta potentials were measured by dynamic light scattering (DLS) (Zetasizer NanoZS90, Malvern Instruments, UK, USA).

4.3. Preparation of in vitro blood clots

We thoroughly mixed 100 µl of 1M saturated solution of $CaCl_2$ with 5 ml of porcine blood (sodium citrate as anticoagulant, Lampire Biological Laboratories, USA) inside a 5 ml syringe at 37 °C, and immediately dispensed the mixture into 5 mm diameter tygon silicone tubing segments. The tubing was then completely sealed using parafilm and incubated at 37 °C in a hot water bath for three hours. The tubing segments containing blood clots were further incubated for another 4 days at 4 °C.[27]

4.4. Fluorescence imaging of model blood clots

Fluorescence imaging of clots were performed using a dark box. Two light emitting diodes (LEDs) delivering excitation light in the range of 700 ± 30 nm were used for illumination. Fluorescent emission from the *in vitro* blood clots was captured using a charge-coupled device (CCD) camera (Pixis 1024B, Roper Scientific, Trenton, NJ, USA) equipped with a long pass filter transmitting wavelengths greater than 810 nm at 60 minutes post incubation with free tPA, NETs, or tPA-conjugated NETs. To prevent pixel saturation, the camera exposure time was set to 90 s for all the images.

4.5. Quantitative analysis of fluorescent images

Acquired fluorescent images were analyzed using ImageJ software. Regions of interests (ROIs) were selected for each blood clot. The averaged total emission intensity (*I**) was calculated as:

$$I^* = \frac{\sum_{j=1}^{k} I_j}{n} \quad (2)$$

where *I* is emission intensity at a given pixel *j* within the ROI, *k* is the total number of pixels in the ROI, and *n* is the number of clots.

4.5. Confocal imaging of model blood clots

The *in vitro* blood clots were incubated with PBS, NETs, or tPA-conjugated NETs for 30 minutes. Blood clots were then washed twice with PBS and stained with the FITC-labeled porcine fibrinogen (Molecular Innovations, Inc., Novi, MI) for 15 minutes at room temperature, and then imaged using a confocal laser scanning microscope (Zeiss LSM 510, Dublin, CA, USA). We used wavelengths of 488 and 633 nm to excite the FITC-labeled porcine fibrinogen, and ICG respectively. The FITC fluorescence signals were collected in the range of 500-550 nm. NIR emission from ICG was collected at wavelengths > 650 nm.

4.6. In vitro thrombolysis experiments

Thrombolysis experiments were performed by placing known amounts of clot in each well of a 24-well plate, which contained PBS (pH~7.4), 500 µl of NETs, 250 and 500 µl of tPA-conjugated NETs, 50 and 100 µl of free tPA respectively. The indicated 250 µl and 500 µl volumes of tPA-conjugated NETs, respectively, contained particles that were fabricated using 61.25 µg/ml and 125 µg/ml of tPA in the reaction buffer during the conjugation process. The corresponding free tPA concentration in the indicated volumes of 50 and 100 µl were 50 and 100 µg/ml, respectively. Clots were then incubated for 120 minutes with each of the agents. The mass of lysed clots was obtained by calculating the difference in mass at 0 and 120 min post-incubation with the indicated agents.[28]

4.7. Statistical analysis

One-way ANOVA analysis of date was conducted using the Origin 9.0 software. We defined statistically significant differences at p value < 0.05.

Acknowledgements

This study was supported in parts by grants from the Bioengineering Center at University of California, Riverside, and the United States National Science Foundation (CBET-1509218). In Figure 1, the structure of tPA was reproduced from protein data bank with ID code 1A5H(http://www.rcsb.org/pdb/explore/explore.do?structureId=1).

Received: ((will be filled in by the editorial staff))
Revised: ((will be filled in by the editorial staff))
Published online: ((will be filled in by the editorial staff))

References

[1] J. G. Romano and R. L. Sacco, *Nat. Rev. Neurol.*, **2015**, *11*, 619.

[2] W. J. Powers, C. P. Derdeyn, J. Biller, C. S. Coffey, B. L. Hoh, E. C. Jauch, K. C. Johnston, S. C. Johnston, A. A. Khalessi, C. S. Kidwell, J. F. Meschia, B. Ovbiagele and D. R. Yavagal, *Stroke*, **2015**, *46*, 3020.

[3] Z. Tang, D. Li, X. Wang, H. Gong, Y. Luan, Z. Liu, J. L. Brash and H. Chen, *J. Mater. Chem. B.*, **2015**, *3*, 977.

[4] I. M. El-Sherbiny, I. E. Elkholi and M. H. Yacoub, *Glob. Cardiol. Sci. Pract.*, 2014, *2014*, 336.

[5] N. Korin, M. Kanapathipillai, B. D. Matthews, M. Crescente, A. Brill, T. Mammoto, K. Ghosh, S. Jurek, S. A. Bencherif, D. Bhatta, A. U. Coskun, C. L. Feldman, D. D. Wagner and D. E. Ingber, *Science*, **2012**, *337*, 738.

[6] J.-P. Chen, C.-H. Liu, H.-L. Hsu, T. Wu, Y.-J. Lu and Y.-H. Ma, *J. Mater. Chem. B.*, **2016**, *4*, 2578.

[7] G. J. Shaw, J. M. Meunier, S.-L. Huang, C. J. Lindsell, D. D. McPherson and C. K. Holland, *Thromb. Res.*, **2009**, *124*, 306.

[8] E. Voros, M. Cho, M. Ramirez, A. L. Palange, E. De Rosa, J. Key, Z. Garami, A. B. Lumsden and P. Decuzzi, *Adv. Func. Mater.*, **2015**, *25*, 1709.

[9] J.-C. Murciano, S. Medinilla, D. Eslin, E. Atochina, D. B. Cines and V. R. Muzykantov, *Nat. Biotech.*, **2003**, *21*, 891.

[10] K. Ganguly, M. S. Goel, T. Krasik, K. Bdeir, S. L. Diamond, D. B. Cines, V. R. Muzykantov and J.-C. Murciano, *J. Pharm. Exp. Ther.,* **2006**, *316*, 1130.

[11] B. Bahmani, D. Bacon and B. Anvari, *Sci. Rep.*, **2013**, *3*, 2180.

[12] J. T. Mac, V. Nuñez, J. M. Burns, Y. A. Guerrero, V. I. Vullev and B. Anvari, *Biomed. Opt. Exp.*, **2016**, *7*, 1311.

[13] P.-A. Oldenborg, A. Zheleznyak, Y.-F. Fang, C. F. Lagenaur, H. D. Gresham and F. P. Lindberg, *Science*, **2000**, *288*, 2051.

[14] H. Zhang, *Biomater. Sci*., **2016**, *4*, 1024.

[15] C.-M. J. Hu, L. Zhang, S. Aryal, C. Cheung, R. H. Fang and L. Zhang, *Proc. Natl. Acad. Sci.,* **2011**, *108*, 10980.

[16] S. C. Stein, K. Ganguly, C. M. Belfield, X. Xu, E. W. Swanson, X. H. Chen, K. D. Browne, V. E. Johnson, D. H. Smith, D. G. LeBold, D. B. Cines and V. R. Muzykantov, *J. Neurotrauma.*, **2009**, *26*, 1585.

[17] C. Minelli, A. G. Shard, *Biointerphases*, **2016**, *11*, 04b306-1.

[18] U. Nobbmann and A. Morfesis, *Mater. Today*, **2009**, *12*, 52.

[19] B. Jung, V. I. Vullev and B. Anvari, *IEEE J. Sel. Top. Quantum Electron.,* **2014**, *20*, 149.

[20] T.-W. Chung, S.-S. Wang and W.-J. Tsai, *Biomaterials*, **2008**, *29*, 228.

[21] S. Koudelka, R. Mikulik, J. Mašek, M. Raška, P. Turánek Knotigová, A. D. Miller and J. Turánek, *J. Control. Release*, **2016**, *227*, 45.

[22] S. Absar, N. Gupta, K. Nahar and F. Ahsan, *J. Thromb. Haemost.*, **2015**, *13*, 1545.

[23] A. S. Drozdov, V. V. Vinogradov, I. P. Dudanov, V. V. Vinogradov, *Sci. Rep.* **2016**, *6*, 28119.

[24] N. Korin, M. Kanapathipillai, B. D. Matthews, M. Crescente, A. Brill, T. Mammoto, K. Ghosh, S. Jurek, S. A. Bencherif, D. Bhatta, A. U. Coskun, C. L. Feldman, D. D. Wagner, D. E. Ingber, *Science* **2012**, *337*, 738.

[25] A. B. Nair, S. Jacob, *J. Basic Clin. Pharm.* **2016**, *7*, 27.

[26] Y. Dong, W. Cao, X. Cheng, K. Fang, F. Wu, L. Yang, Y. Xie, Q. Dong, *Stroke Vascular Neurol.* **2016**, *1*, 115.

[27] J. T. Sutton, N. M. Ivancevich, S. R. Perrin, Jr., D. C. Vela and C. K. Holland, *Ultrasound Med. Biol.,* **2013**, *39*, 813.

[28] D. Suo, Z. Jin, X. Jiang, P. A. Dayton and Y. Jing, *Appl. Phys. Lett.,* **2017**, *110*, 023703.

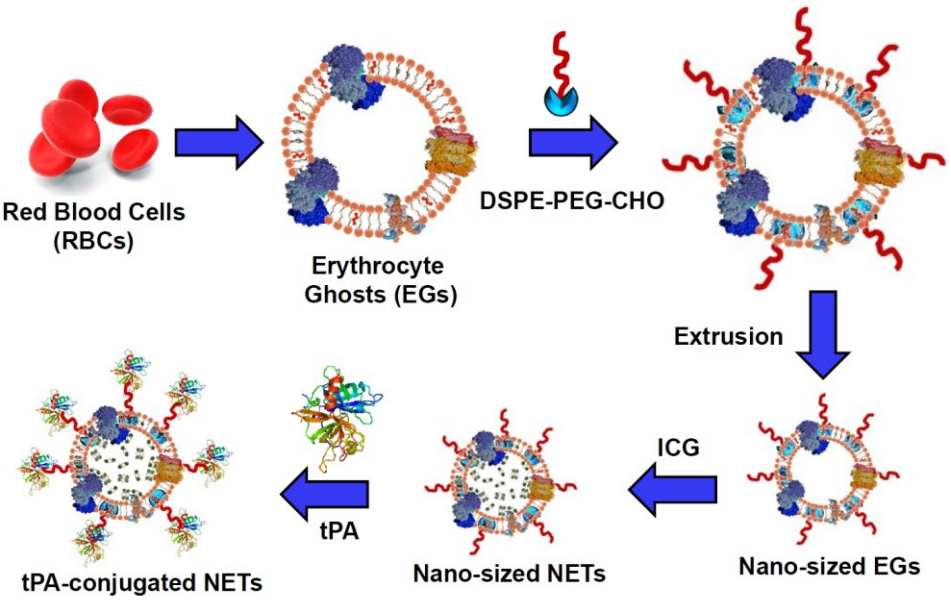

Figure 1. Schematic representation for fabrication of tPA-conjugated NETs.

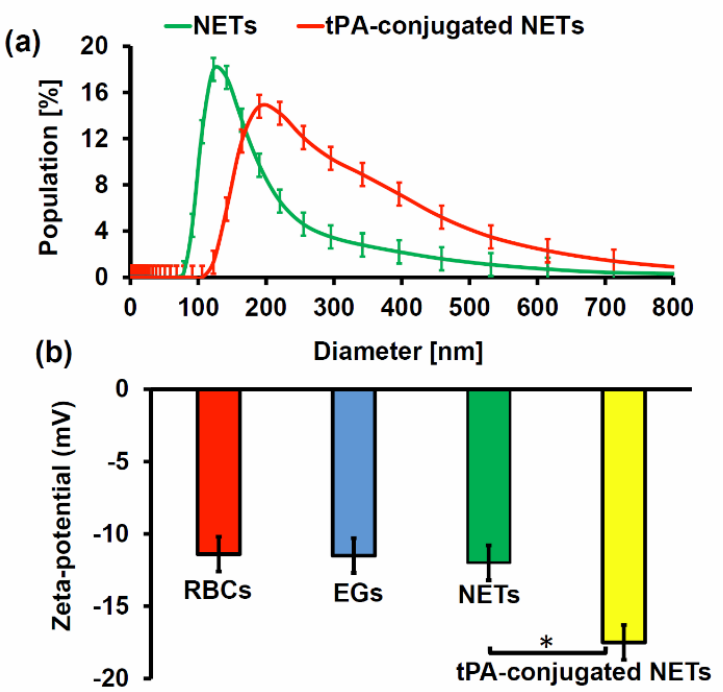

Figure 2. (a) Dynamic light scattering (DLS)-based measurements of hydrodynamic diameters for NETs and tPA-conjugated NETs formulations in 1X PBS. Each measurement was repeated using at least three samples. We present the mean of each measurement where the errors bars represent standard deviations from the mean values. We fitted Lorentzian functions to the measured diameter distributions. (b) Zeta-potentials for native RBCs, nano-sized EGs, NETs and tPA-conjugated NETs

formulations. All measurements were recorded in 1X PBS. Error bars represent the standard deviation for three independent measurements. Asterisk indicates statistically significant differences ($p < 0.05$) between the indicated pairs.

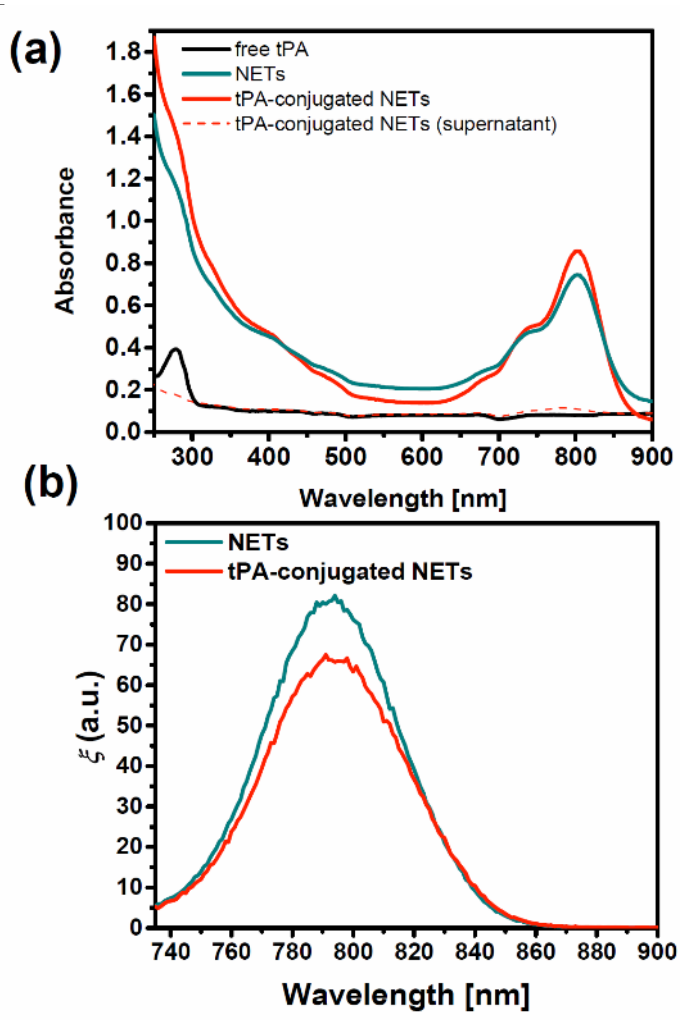

Figure 3. (a) Absorption spectra of free tPA, NETs and tPA-conjugated NETs. The red dashed trace indicates the supernatant collected after ultracentrifugation during the fabrication of tPA-conjugated NETs. (b) Normalized fluorescence emission spectra (□) (please see equation (1) in

Experimental Section) of NETs and tPA-conjugated NETs in response to photo-excitation at 720 nm. All the measurements were recorded in 1X PBS (≈ 310 mOsm). Concentrations of free tPA, and that in the reaction buffer for conjugation of NETs were 100 and 125 μg/ml, respectively.

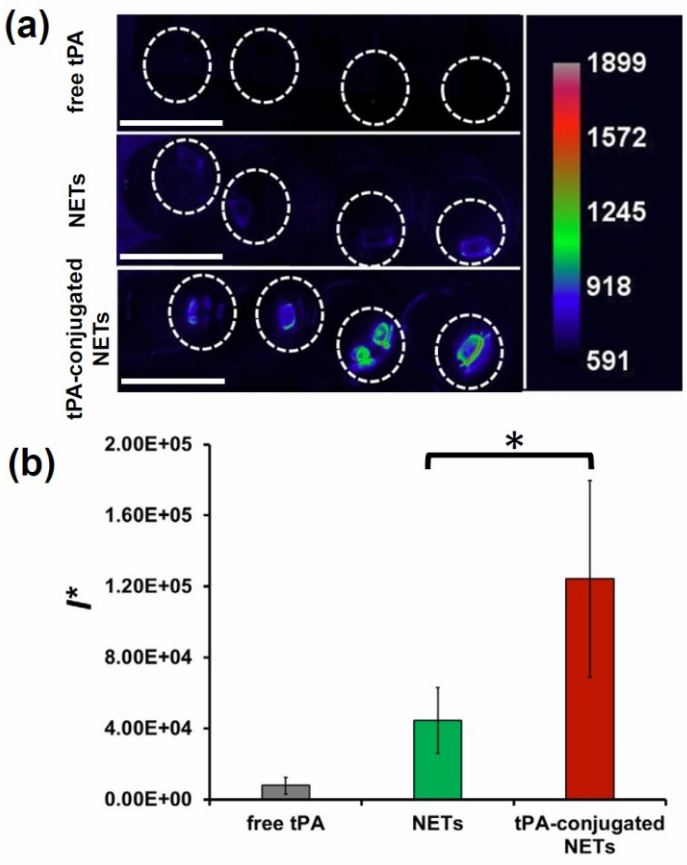

Figure 4. Fluorescent images of blood clots at one hour post-incubation with various agents (Excitation wavelength = 710 nm, and emission > 760 nm recorded). The regions of interests (ROIs) of model blood clots are within circles delineated by dashed white traces. Concentrations of free tPA, and that used in fabrication of tPA-conjugated NETs were 50 and 61.25 μg/ml, respectively.

Concentration of ICG used in fabrication of NETs and tPA-conjugated NETs was 15 μM. The falsely-colored scale bar on the right is associated with the emission intensity of ICG encapsulated within NETs or tPA-NETs. The scale bar for physical dimension is 3 cm. (b) Averaged total emission intensity (I^*) of blood clots (please see equation (2) in Experimental Section) from the ROIs for various agents. Asterisk indicates statistically significant differences ($p < 0.05$) between the indicated pairs.

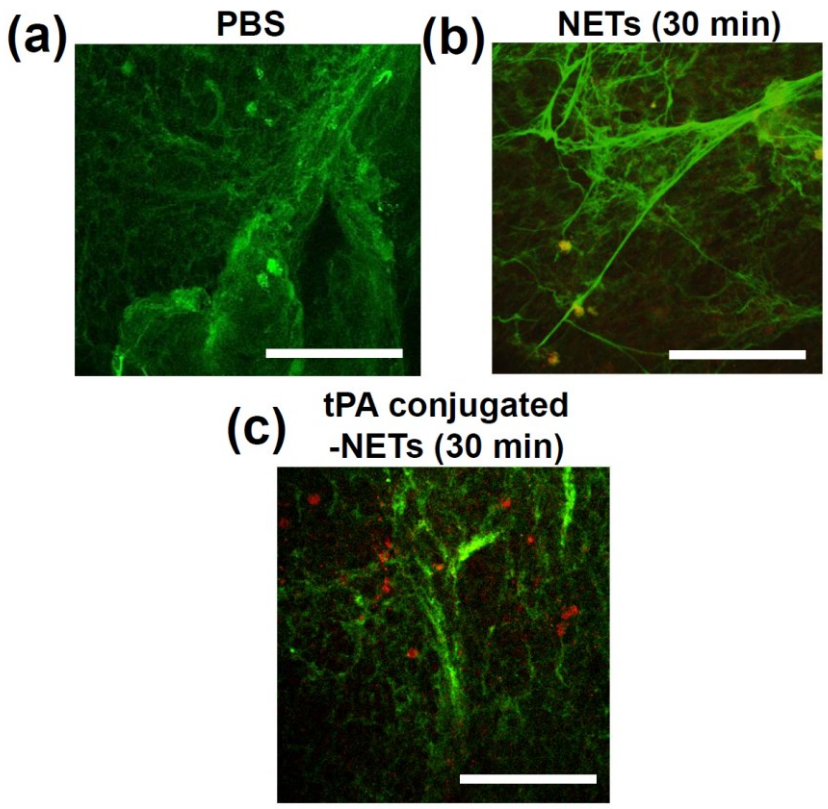

Figure 5. Confocal fluorescent microscopy images of *in vitro* model blood clots incubated with different agents: (a) PBS, (b) NETs, and (c) tPA conjugated NETs for 30 min. Concentration of tPA used for fabrication of tPA-conjugated NETs in the reaction buffer was 125 μg/ml. The fibrin network of the model blood clot was stained with FITC-labeled porcine fibrinogen and falsely colored as

green. NIR fluorescence emission associated with ICG was falsely colored in red. The overlay of green and red was shown in yellow. Each scale bar is 50 µm.

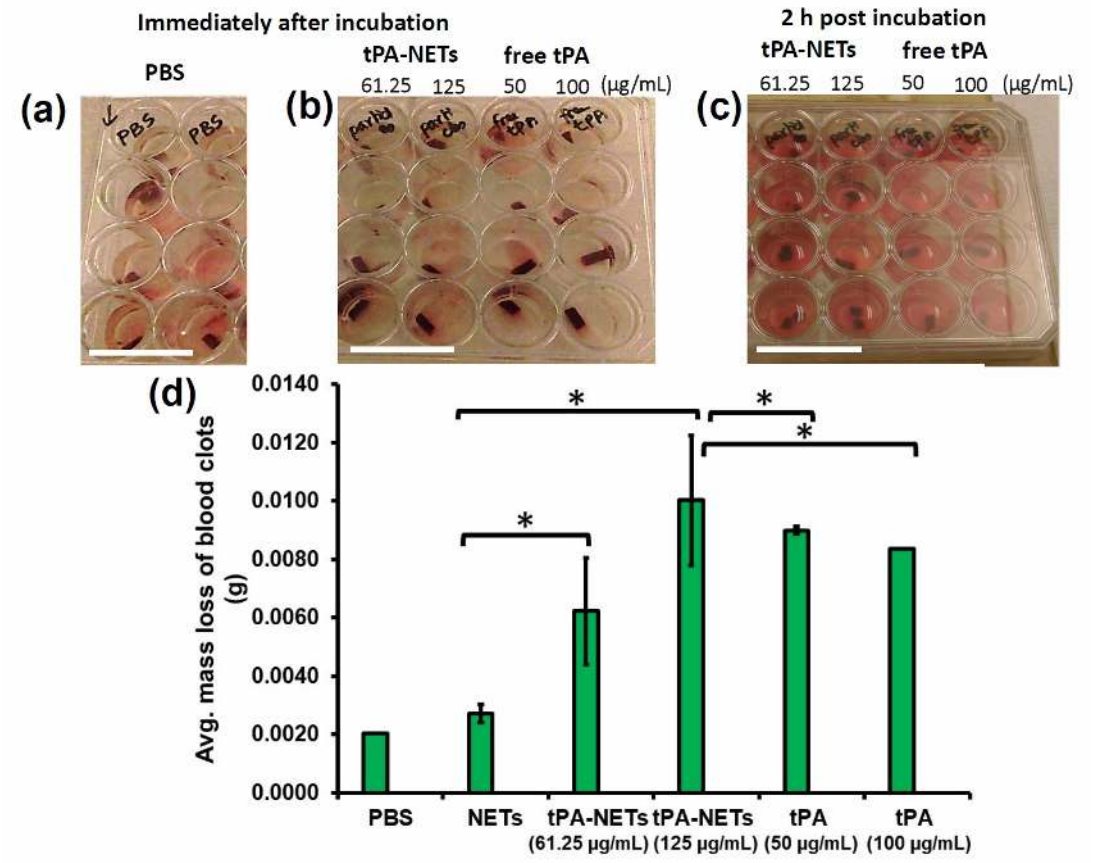

Figure 6. Representative photographs of *in vitro* blood clot model (a-c). Panels (a) and (b) correspond to the blood clot models immediately after incubation in PBS alone, and PBS containing tPA-conjugated NETs and free tPA, respectively. Panel (c) corresponds to the blood clots two hours

post incubation with tPA-conjugated NETs and free tPA. In panels (b) and (c), the first two columns correspond to the blood clots treated with tPA-conjugated NETs, and the last two columns to clots treated free tPA. The scale bars for physical dimensions in panels (a-c) are 3 cm. (d) Average mass loss of model blood clots at two hours post incubation with PBS, tPA-conjugated NETs, and free tPA. Error bars represent the standard deviation for four independent measurements. Concentration values of free tPA were 50 and 100 μg/ml. We used tPA concentration values of 61.25 and 125 μg/ml in reaction buffers to fabricate the tPA-conjugated NETs. Asterisks indicate statistically significant differences ($p < 0.05$) between the indicated pairs.

We report the first proof-of-principle demonstration of a new theranostic nano-structured system composed of erythrocyte-derived vesicles encapsulating the FDA-approved near infrared fluorophore, indocyanine green (ICG), and conjugated with FDA-approved drug, tissue plasminogen activator (tPA) for simultaneous fluorescence imaging and thrombolysis of blood clots.

Keywords: indocyanine green, ischemic stroke, tissue plasminogen activator

Raviraj Vankayala[a], Samantha R. Corber[b], Jenny T. Mac[c], Masaru P. Rao[a,b,d], Mohammad Shafie[e], Bahman Anvari[a,b,c]

Erythrocyte-Derived Nanoparticles as a Theranostic Agent for Near Infrared Fluorescence Imaging and Thrombolysis of Blood Clots